



Contents lists available at ScienceDirect

Arabian Journal of Chemistry

journal homepage: www.ksu.edu.sa

Original article

Silver (Ag) doped graphitic carbon nitride (g-C₃N₄) photocatalyst for enhanced degradation of Ciprofloxacin (CIP) under visible light irradiationIjlal Idrees^{a,1}, Abdul Razzaq^{a,1,*}, Muhammad Zafar^{b,1,*}, Adeel Umer^c, Faiza Mustafa^d, Fahad Rehman^a, Woo Young Kim^{e,*}^a Department of Chemical Engineering, COMSATS University Islamabad, Lahore 54000, Pakistan^b Institute of Energy and Environmental Engineering, University of the Punjab, Lahore 54590, Pakistan^c School of Chemical and Materials Engineering (SCME), National University of Sciences and Technology (NUST), H-12, Islamabad, Pakistan^d Department of Physics, COMSATS University Islamabad, Lahore 54000, Pakistan^e Department of Electronic Engineering, Faculty of Applied Energy System, Jeju National University, Jeju-si 63243, Jeju Special Self-Governing Province, Korea

ARTICLE INFO

Keywords:

Doped Photocatalyst

Visible Light activity

Ag doping

Graphitic carbon nitride (GCN)

Ciprofloxacin (CIP) degradation

ABSTRACT

Pharmaceutical industry wastewater is causing an increased risk of resistant pharmaceutical micropollutants (PMP) e.g. antibiotic resistant bacteria (super bug) in the ecosystem. Amongst variety of wastewater treatment approaches, Advanced oxidation processes (AOPs) employing photocatalysis provides a cost-effective and sustainable approach for fixation of PMP in an economical and efficient manner to counter the potential risks. Until today, tremendous efforts have been made to trig the performance of photocatalytic wastewater treatment, with the key focus on development of cost-effective, efficient and a moderately stable photocatalyst. Such attempts succeeded with different types of photocatalysts using different synthesis techniques. In recent years, graphitic carbon nitride (GCN) has emerged as one of the cost effective, moderately stable, nontoxic and efficient photocatalyst, and has been scarcely studied specifically for pharmaceutical micropollutants (PMPs) degradation. Hence, considering these factors alongside the facile synthesis and moderate optical absorption of GCN, an effort was made in the present work with effective customization of GCN i.e. silver (Ag) doping to extend light absorption in visible light range which may enhance the photocatalytic performance for Ciprofloxacin (CIP) degradation. The optimization of photocatalytic performance was executed with varied Ag dopant content to obtain an optimum sample with supreme photocatalytic activity for the maximum degradation of CIP, a common antibiotic. The best Ag-doped GCN sample (0.1 AGCN) exhibits a photocatalytic degradation efficiency of 84%, which is 2.15 times greater than pure GCN (39%). The obtained results showed that the strategy of Ag doping substantially enhances the photocatalytic performance, thus offering an efficient mean for developing visible light active photocatalyst for PMP removal and encouraging further research. The photocatalytic performance of the prepared samples was evaluated by degradation of CIP under visible light irradiation. Several characterization techniques were used to characterize and analyze the prepared samples, such as X-ray diffraction (XRD), Scanning electron microscopy (SEM), Raman spectroscopy, Fourier Transform Infrared (FTIR) spectroscopy, UV Visible absorption, and Photoluminescence (PL) spectroscopy.

1. Introduction

An increase in world population and human activity on the planet has triggered and progressively encouraged the contamination of the environment via different types of organic and inorganic pollutants (Belhaj et al., 2015). Out of the many environmental risks, water pollution, and contamination is one of the major and potential challenge desired to be fixed on a prime basis (Schweitzer and Noblet, 2018).

Water contamination is mainly caused by improper disposal of wastewater from various industries such as textile, agricultural, fertilizer, leather and tannery, cosmetics and pharmaceutical etc. Hence, rapid industrialization and development improve human lifestyle and comfort, on contrary, it comes with severe environmental issues directly influencing human life, wildlife, aquatic habitats, climatic changes, and global warming (Demir et al., 2014). Amongst various industries, pharmaceutical industry contributes vitally to water pollution via

* Corresponding authors.

¹ These authors contributed equally to this work.

improper disposal of certain important drugs such as antibiotics, anti-septics, steroids, and hormones (Chander et al., 2016). The excessive and/or undesirable medicines are disposed directly to sewage water, affecting the environment directly, which may lead to stable, and complex nature of the pharmaceutical micropollutants (PMP) pertaining for a long duration. Moreover, PMP can penetrate the surface and groundwater, portraying a major threat to human life and the ecosystem. Thus, pharmaceutical micropollutants (PMP) are considered a potential threat to the ecosystem because of their recurrent usage and presence in high concentrations among various environmental bodies (Verlicchi et al., 2012). The PMP, including antibiotics, are mostly complex organic compounds in nature with diverse physiochemical and beneficial properties (Kümmerer, 2009). Along with their countless benefits, these PMPs, specifically antibiotics, are devastating the ecology of developing countries (Rehman et al., 2015). Antibiotics have also increased the number of antibiotic-resistant bacteria termed as "SUPER BUG" in the environment. It is estimated that around 700,000 deaths around the world are caused by such bacterial infections (Abromaitis et al., 2022). Recently, during the COVID-19 pandemic, the use of pharmaceutical and personal care products increased by 80% between 2020 and 2022, with increased consumption and releasing of pharmaceutical drugs and antibiotics (Chen et al., 2021; Conceicao et al., 2023). Around the world, 667 million people were affected by COVID-19. Due to such a vast level of effects in almost every part of the world, the use of pharmaceutical drugs and antibiotics has greatly increased which has led to biohazardous effects on aquatic and land environments. Therefore, after such a calamity, the presence of PMPs in the ecosystem is inevitable, and strategies must be developed for their removal from the environment (Khan et al., 2023; Parasuraman et al., 2023b).

Among the antibiotic drugs, ciprofloxacin (CIP), introduced in the 1980s, a second-generation fluoroquinolone antibiotic with a quinolone structure and piperazine part, is the most widely used to treat many bacterial infections and illnesses through antimicrobial action (Shehu Imam et al., 2018). It is established that along with other PMPs, ciprofloxacin is present in wastewater sources near relevant industries, hospitals, clinics, and sewage waste. Further, CIP possesses more complex segmented adsorption in the sediments, which are difficult to remove from the environment (Ashfaq et al., 2019). Hence, it is necessary to purify water from such persistent PMP at an early stage by employing a more sustainable and viable treatment approach that can be easily implemented by these pharmaceutical industries for a better ecosystem (Sirés and Brillas, 2012).

Various treatment methodologies/approaches for fixing/degrading the PMP include ozonation, membrane technology, adsorption, advanced oxidation processes (AOPs), chemical and biological treatments (Eniola et al., 2022). Among these techniques, chemical treatment offers coagulation-flocculation method (Ghazal et al., 2022). Activated carbon and cellulose membranes are also widely used to remove CIP from wastewater, where 27% elimination of CIP was observed using cellulose membrane (Bera et al., 2022; de Ilurdoz et al., 2022). Advanced oxidation processes (AOPs), including electrochemical oxidation (EO), ozonation, and Fenton process (FP), are the most promising treatment technologies used worldwide for wastewater treatment. AOPs based on ultraviolet radiation (UV/H₂O₂) technology for CIP removal from wastewater are an alternative to conventional AOPs (An et al., 2010). Biological treatment is also attractive treatment technology in which Anaerobic Digestion (AD) is the most prominent method under the anaerobic method, whereas the Biological Aerated Filter system (BAF) is the most widely used technique under the aerobic method (Lakatos, 2018).

Under the domain of AOPs, photocatalytic wastewater treatment employs semiconductor materials (acting as a photocatalyst) which become active under light irradiation, a free source of energy, charges are generated at the photocatalysts surface which reacts with the target pollutant ultimately oxidizing into less or nonhazardous products. Hence photocatalysis provides a cost effective and efficient way to fix

the PMP in wastewater.

Until today, an extensive amount of research has been done for the development of photocatalytic materials mainly metal oxides including TiO₂, ZnO, Fe₂O₃, WO₃, Cu₂O, and LaFeO₃ etc. These photocatalysts possess key benefits of low cost, favorable redox potential, improved chemical-physical stability, and friendly behavior towards environment (Aruljothi et al., 2023; Bahnemann, 2004; Bhuvanewari et al., 2021). Besides their pros, the cons of these photocatalysts include photo-corrosion effect causing lower stability during photocatalysis, and limited light absorption due to wider band gap, restricted to UV light region which comprises 4–5% of terrestrial light (Lee et al., 2016; Parasuraman et al., 2023a). As an example, case of TiO₂ which is considered as a standard photocatalyst, absorbs only UV light due to its wide band gap (3.2 eV), and to some extent recombination of photogenerated electron and hole pairs, thus limiting its ability to perform for a wider scale of applications (Bhuvanewari et al., 2023; Lee and Park, 2013). Therefore, a necessity to synthesize visible light active photocatalyst, with minimized photogenerated carrier recombination arises with specific application of wastewater treatment in a cost-effective manner.

Visible light active photocatalysts have got recognition among researchers as a major portion of sunlight is visible light (approx. 40–45%), and can be utilized effectively in photocatalytic applications. Among visible light active photocatalysts, graphitic carbon nitride (GCN) in the last decade has gained enormous attention due to its simple synthesis, stable and non-toxic behavior, and band gap falling within visible light range (Zheng et al., 2016). GCN is a material with an average band gap of 2.9 eV, and decent visible light response up to 460 nm (Du et al., 2012). With these features of low cost, simplistic preparation, good chemical stability, and band gap, GCN is an optimal photocatalyst to be used in photocatalytic applications. Despite of admirable advantages, photocatalytic performance is still restricted mainly due to quick recombination of photogenerated electron-hole pairs, low surface area, and insufficient visible light absorption (Xu et al., 2018). In literature, certain modification approaches are reported for GCN modification with the aim of enhanced performance such as metals and non-metals doping, GCN exfoliation, sensitizers loading, coupling with other photocatalytic materials resulting in heterojunction like Z-scheme etc. (Jiang et al., 2017; Kumar et al., 2020; Li and Shi, 2016; Rabbani et al., 2023; Raizada et al., 2020; Shanmugam et al., 2023; Wen et al., 2018). The photocatalytic performance enhancement by simply doping of GCN is one of the uncomplicated and effective strategies for narrowing of band gap leading to increased optical absorbance and active sites. Furthermore, the dopants in the GCN network also inhibit charge recombination and increase surface area. Consequentially to improve the photocatalytic performance of GCN, established focused is on enhancement of optical absorption, minimization of photoexcited charges recombination and improved surface area.

Thus, being inspired by the imperative effects of doping strategy, the present work portrays a facile synthesis approach for silver (Ag) doped GCN and its application for CIP, a potential PMP, degradation. Ag metal is doped into GCN, narrowing down its band gap, in turn extending its visible light absorption with outcome of improved photocatalytic activity for CIP degradation. The Ag dopant concentration is varied and optimized with respect to CIP degradation. The compelling aspect of Ag doped GCN is its superior photocatalytic performance under 5 W LED white light irradiation. Additionally Ag doping also suppresses the photogenerated charge recombination and variation in morphology.

2. Experimental section

2.1. Chemicals and reagents

Urea (NH₂CONH₂ ≥ 99%) was purchased from PENTA CHEMICALS UNLIMITED and was used for synthesis of GCN. Silver nitrate (AgNO₃, ACS grade ≥ 99%) was purchased from VWR CHEMICALS and was used for doping. Both chemicals were used as obtained without any

modification. Deionized (DI) water was used as a solvent and obtained from Aqua Flow (Made in Taiwan) reverse osmosis water purifier system for washing throughout the experimentation. Ciprofloxacin (CIP) antibiotic was obtained from Pakheim International Pharmaceuticals Pvt. Limited and used as a targeted pollutant to evaluate photocatalytic activity.

2.2. Synthesis of pure graphitic carbon nitride (pure GCN)

Pure graphitic carbon nitride (pure GCN) was prepared using a conventional thermal polycondensation process. In brief, 20.0 g of urea was taken in a 100.0 ml ceramic crucible and placed in a muffle furnace at 550 °C for 3 h in static air. The obtained light-yellow powder after the completion of the process was taken out, well-grounded using mortar and pestle, washed using centrifugation, and dried at 70 °C overnight. The obtained product was given the name pure graphitic carbon nitride (pure GCN) (Das et al., 2018; Guo et al., 2020, 2017; Zhang et al., 2013).

2.3. Synthesis of silver doped graphitic carbon nitride (x-AGCN)

Silver (Ag) doped GCN was synthesized in a similar manner as pure GCN was synthesized with minor modification. In brief, 10.0 g of urea with a specified amount of silver nitrate (AgNO_3) was dissolved in 50.0 ml D.I water via stirring for 30.0 min using a magnetic stirrer. After proper dissolution, an alight milky mixture obtained, is evaporated on a hot plate under continuous stirring at 70 °C. The white crystalline dried crust obtained in the beaker was collected and transferred to a ceramic crucible, which is subjected to a thermal polycondensation process (like pure GCN) in a muffle furnace at 550 °C (3 h). The as-prepared powder was collected, grounded, washed, filtered, and then subjected to overnight drying in an oven at 70 °C. Five different samples of silver (Ag) doped GCN were prepared by varying the amount of silver nitrate (AgNO_3) = 0.05 g, 0.07 g, 0.1 g, and 0.13 g to obtain optimal photocatalysts based on photocatalytic performance in accordance to CIP degradation. The different samples prepared were designated as x-AGCN (where x = 0.05, 0.07, 0.1, and 0.13 g of AgNO_3).

2.4. Materials characterization

Crystallinity of the prepared samples was investigated by obtaining X-ray diffraction (XRD) patterns of the prepared samples using a PANalytical X-pert Powder diffractometer, Pro DY38059, employing $\text{Cu K}\alpha$ radiations of 0.15406 nm. The presence of inorganic and organic compounds and structural bonds was identified using a Fourier transform infrared spectroscopy (FTIR THERMO NICOLET 6700 USA). The electron-hole pairs recombination are studied using Photoluminescence (PL) spectroscopy. The prepared sample's chemical structure, crystallinity, and molecular interactions were investigated by obtaining respective Raman spectra. Raman and photoluminescence (PL) were examined with the laser excitation source of 514 nm and 457 nm, respectively, by InVia Raman Microscope by RENISHAW UK. The prepared samples surface morphology and elemental composition were determined by obtaining images via Scanning electron microscopy (SEM) with the help of JSM-6490A equipment possessing built-in function of energy dispersive X-ray spectroscopy (EDX) for elemental composition analysis. The optical absorption of the prepared samples was investigated by obtaining UV-VIS absorption of the dilute suspensions of samples using a UV-1602 spectrometer provided by Biotechnology Medical Services (BMS).

The band gaps (E_g) of the prepared samples were estimated by using the Tauc's relation (Sarwar et al., 2023):

$$(\alpha h\nu)^n = A(h\nu - E_g) \quad (1)$$

where α is the molar absorption coefficient, A is a constant, E_g is the average band gap of the material, n is the number of transitions, and $h\nu$

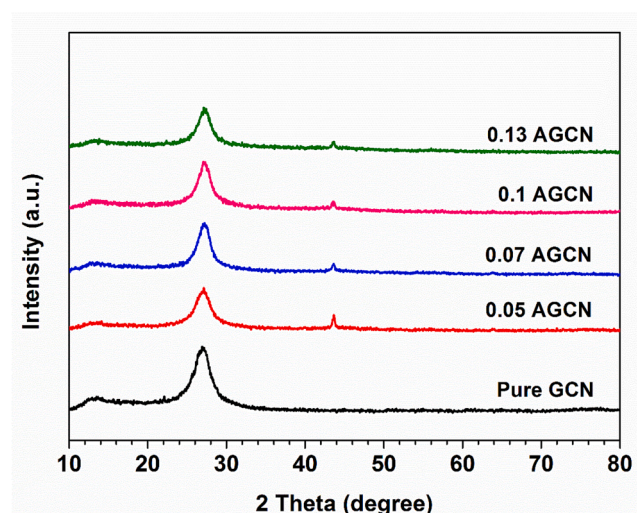


Fig. 1. XRD patterns of pure GCN and x-AGCN (where x = 0.05, 0.07, 0.1, and 0.13 g of AgNO_3).

is the photon energy.

2.5. Photocatalytic activity measurement

The prepared photocatalysts activity was evaluated by the degradation of Ciprofloxacin (CIP) micropollutant under visible light irradiation. The photocatalyst samples include pure GCN, 0.05-AGCN, 0.07-AGCN, 0.1-AGCN, and 0.13-AGCN. Typical, 10.0 ppm CIP solution was made in 100.0 ml D.I water, and its UV-VIS spectrum was determined for the photocatalytic degradability comparison with dark and under light irradiation. The solution was then poured into a photocatalytic glass reactor with a 5 W visible light source and magnetic stirrer. The solution was allowed to stir for 10 mins for the homogeneous dispersion of the micropollutant. Then 0.2 g of the photocatalyst was added to the photocatalytic reactor containing CIP (10 mg/L). The mixture was kept in the dark under continuous stirring for 1 h to achieve adsorption-desorption equilibrium. After 1 h, the CIP sample was taken and centrifuged at 5000 rpm for 5 min. and its UV-VIS spectrum was obtained. Now, the light source was irradiated on the reactor, and CIP samples were taken from the reactor after every 15 min of reaction. The light irradiation was performed for 2 h. These samples were centrifuged, and their UV-VIS spectra were determined. A similar approach was used for finding the degradation data of CIP for 0.05-AGCN, 0.07-AGCN, 0.1-AGCN, 0.13-AGCN. The degradation efficiency, and normalized concentration vs. time were obtained using the following equation (Krýsa et al., 2000):

$$\text{Rate of degradation} = \frac{C_0 - C_T}{C_0} \times 100 \quad (2)$$

where C_0 is the initial concentration of CIP at time, $t = 0$ min.,

C_T is the concentration of CIP at a certain time i.e., after 1 h of dark condition and after every 15 min. during light irradiation period.

The rate of the reaction for CIP degradation is analyzed by a pseudo first-order kinetic model. The rate constant equation for this model is given as (Chakrabarti and Dutta, 2004):

$$kt = \ln\left(\frac{C_0}{C_t}\right) \quad (3)$$

where " C_0 " is the initial concentration of CIP, and " C_t " is the concentration of CIP after time " t ".

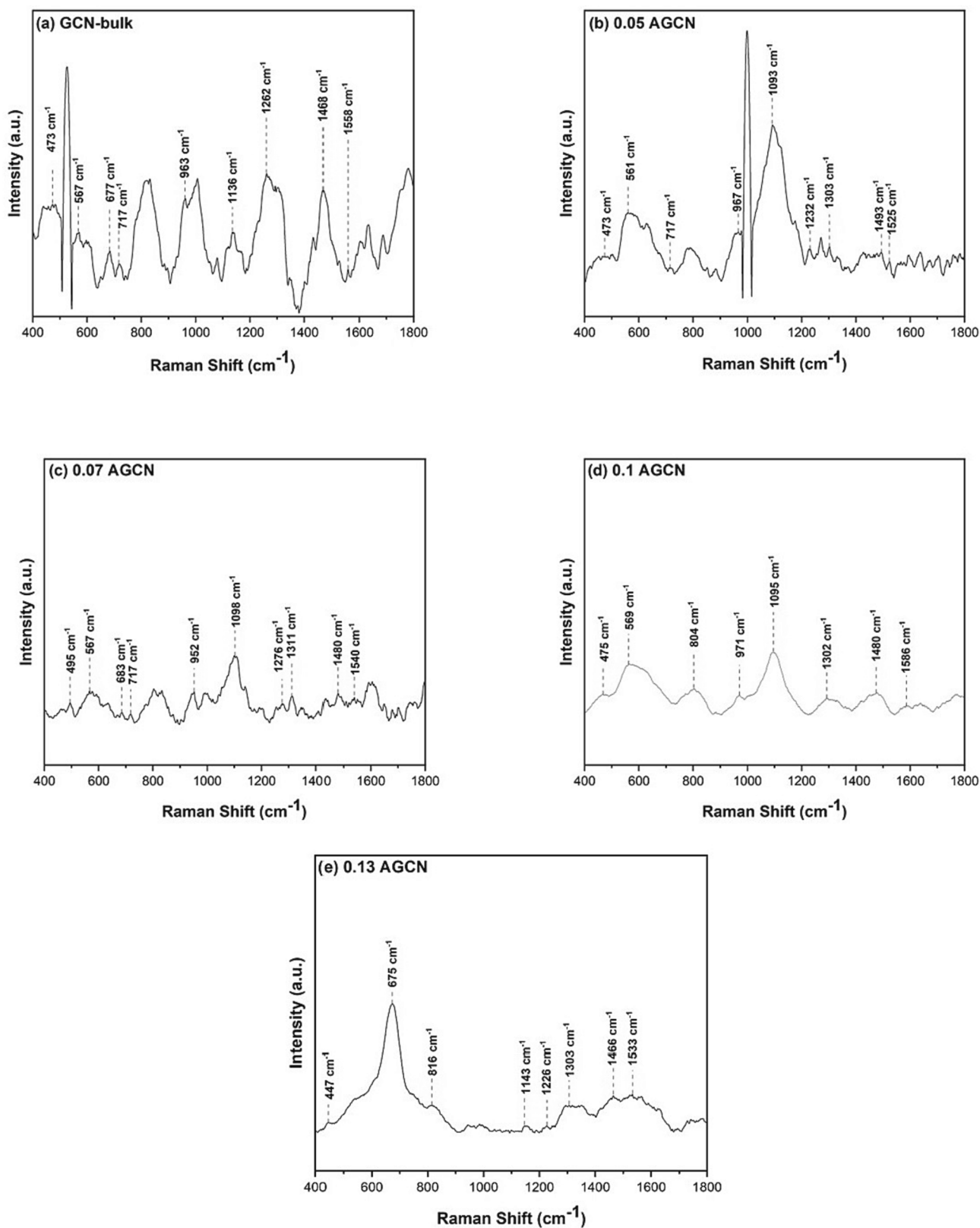


Fig. 2. Raman spectra of (a) pure GCN, (b) 0.05 AGCN, (c) 0.07 AGCN, (d) 0.1 AGCN, and (e) 0.13 AGCN samples.

3. Results and discussion

3.1. Crystallinity analysis

The crystallinity of the prepared samples was investigated by

obtaining their X-ray diffraction (XRD) patterns. Fig. 1 exhibits the XRD pattern of the pure GCN and Ag doped GCN i.e. x-AGCN samples, displaying a small humpy peak appearing around 2θ values of 13.0° and a distinct characteristic peak appearing around 27.5° . The smaller peak can be attributed to (100) plane of oriented melon units, providing

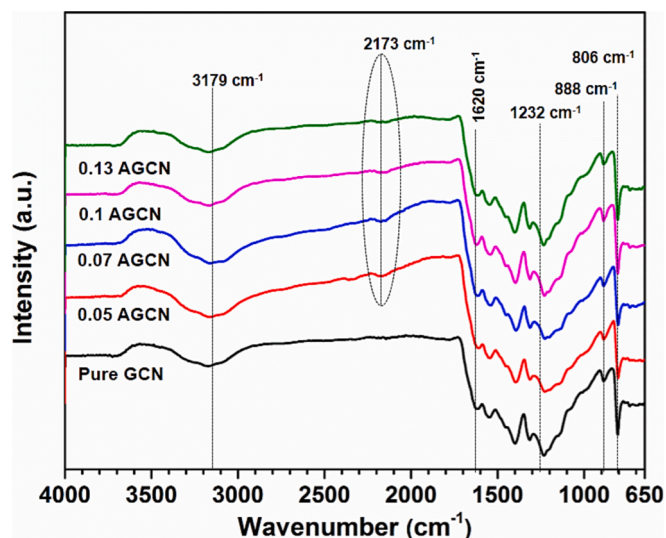


Fig. 3. Fourier transform infrared (FTIR) spectra for pure GCN and *x*-AGCN (where *x* = 0.05, 0.07, 0.1, and 0.13 g of AgNO₃).

primary framework to GCN, whereas second prominent peak is associated to (002) plane representing the stacked graphitic content of crystalline GCN (Bu et al., 2014; Ge et al., 2011; Han et al., 2014; Liu et al., 2012; Sridharan et al., 2013; Tian et al., 2014). It can be noticed that all the samples i.e., pure GCN and *x*-AGCN exhibit significantly these two peaks corresponding to crystalline GCN, suggesting Ag dopant do not disturb the molecular structure and retained the main phase of GCN. However, upon doping Ag into GCN, a small peak is observed appearing at 43.7° which provides a clue of successful Ag doping into GCN and its crystalline nature (Luo et al., 2017; Pham et al., 2022, 2021; Xu et al., 2014; Zhang et al., 2014; Zhao et al., 2018).

3.2. Raman spectroscopy

Vibrational modes in a GCN molecular structure are investigated with Raman Spectroscopy. Fig. 2 illustrates the Raman Spectra of pure GCN and *x*-AGCN samples. The Raman spectrum for pure GCN (Fig. 2a) shows the vibrational signals of CN heterocycle appearing at a wavenumber of 473 cm⁻¹ (Li et al., 2017). However, for Ag doped samples i.e. *x*-AGCN samples (Fig. 2b–e), the respective CN heterocycle signal is observed with shifted wavenumber values such as at 473 cm⁻¹ for 0.05 AGCN, 495 cm⁻¹ for 0.07 AGCN, 475 cm⁻¹ for 0.1 AGCN, and 447 cm⁻¹ for 0.13 AGCN (Jiang et al., 2016; Li et al., 2017). Such slight shifting indicates Ag doping well into the GCN structure.

The in-plane balanced stretching vibrations of heptazine and tri-s-triazine heterocyclic structure are observed in all samples within the range of 500 cm⁻¹–600 cm⁻¹, and 1090 cm⁻¹–1150 cm⁻¹, respectively.

The pure GCN sample doesn't exhibit any characteristic Raman peak of Ag, however, *x*-AGCN samples depict the Ag peaks appearing at 1303 cm⁻¹ for 0.05 AGCN, 1311 cm⁻¹ for 0.07 AGCN, 804 cm⁻¹, and 1302 cm⁻¹ for 0.1 AGCN, 816 cm⁻¹ and 1303 cm⁻¹ for 0.13 AGCN (Bai et al., 2014; Prabakaran and Pillay, 2021). The peaks appearing within the range of 500 cm⁻¹–600 cm⁻¹, 700 cm⁻¹–800 cm⁻¹, and 1200 cm⁻¹–1300 cm⁻¹ shows A1 vibration pattern of bulk GCN tri-s-triazine group (Liu et al., 2010). The peak at 677 cm⁻¹ shows a ring breathing mode 2 of the triazine ring, suggesting deformation in the triazine ring of pure GCN. Similar peaks are found in all other samples from 600 cm⁻¹–700 cm⁻¹, except 0.1 AGCN, which shows a low rate of deformation in the sample (Liu et al., 2010). Ring breathing mode 1 of the tri-s-triazine ring is present in all samples at 717 cm⁻¹, and within 900 cm⁻¹–1000 cm⁻¹ (Hu et al., 2015). The peaks appearing within 400 cm⁻¹–500 cm⁻¹ and 900 cm⁻¹–1000 cm⁻¹ are prominent in pure GCN, whereas they are weaker in *x*-AGCN samples, suggesting structural deformation due to the addition of Ag dopant (Pawar et al., 2015). The peaks within 1200 cm⁻¹–1300 cm⁻¹ and 1500 cm⁻¹–1600 cm⁻¹ represent the defects in the graphite structure and enlarging modes of C=N bond. The disordered phase and imperfections in the graphite layer of sp³ atoms represented by ring modes of the A1 pattern of pure GCN (D band) are exhibited by peak at 1468 cm⁻¹. Whereas, the graphite-like structure of E_{2g} corresponding to sp² carbon-carbon bonds in the chains (G band) appears at 1558 cm⁻¹ (Kudin et al., 2008). For 0.05 AGCN, the D and G bands appear at 1493 cm⁻¹ and 1525 cm⁻¹; for 0.07 AGCN, the D and G bands are at 1480 cm⁻¹ and 1540 cm⁻¹; for 0.1 AGCN, the D and G bands are at 1480 cm⁻¹ and 1586 cm⁻¹, and for 0.13 AGCN the D and G bands are at 1466 cm⁻¹ and 1533 cm⁻¹ (Kora and Arunachalam, 2012). The intensity of D band is too much higher than G band for pure GCN samples, indicating the presence of defects and the formation of graphite structure, while in *x*-AGCN samples, the intensity of both D band and G band is reduced, indicating fewer defects and disorders possibly due to Ag doping (Guo et al., 2022b).

3.3. Fourier transform infrared spectroscopy (FTIR)

FTIR spectra of pure GCN and *x*-AGCN samples (0.05-AGCN, 0.07-AGCN, 0.1-AGCN, 0.13-AGCN) are shown in Fig. 3. All samples show a broad band at 3179 cm⁻¹, which can be attributed to surface O–H stretching vibrations (Bojdys et al., 2008). The stretched carbon nitrile (CN) arrangements depicted by characteristic stretching of C–N heterocycles can be observed in all samples within wavenumber range of 1200–1630 cm⁻¹. The winding vibrations of carbon and nitrogen atoms comprising the triazine structure are depicted by vibration at 888 cm⁻¹, whereas the wagging and twisting vibrations of tri-s-triazine ring are represented by a peak at 806 cm⁻¹ (Li et al., 2009). The intensity of all the peaks mentioned above is relatively decreased in Ag doped samples i.e. *x*-AGCN samples, indicating structural deformation due to the addition of Ag dopant. This may lead to the deformation of sp² C–N bonds existing in triazine ring due to Ag dopant, which might be

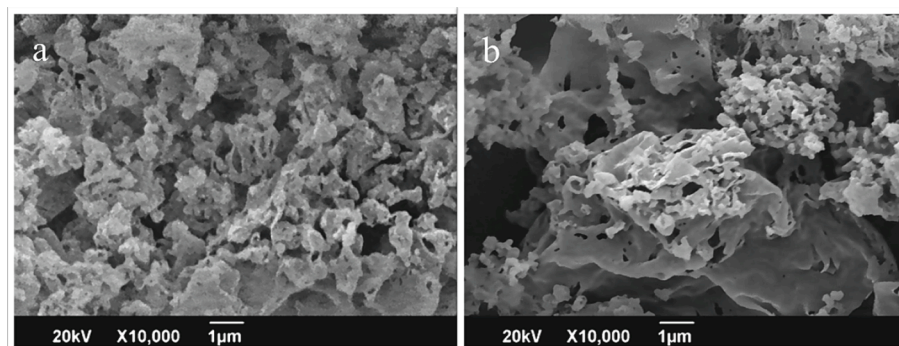
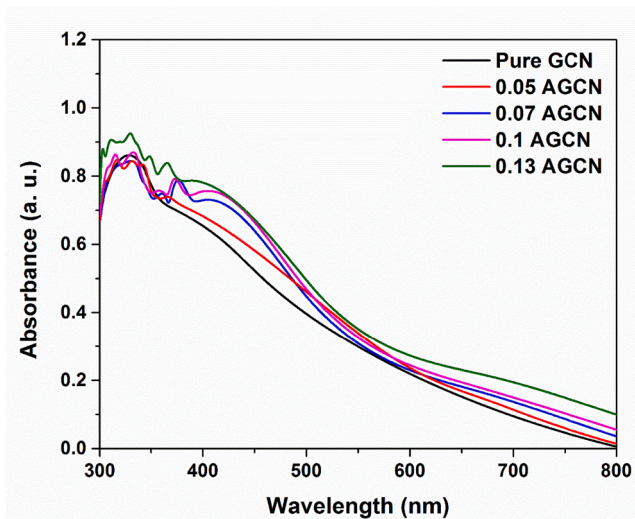


Fig. 4. SEM images of (a) pure GCN, and (b) 0.1-AGCN samples.

Table 1

The atomic concentration of pure GCN and 0.1 AGCN by EDX spectroscopy.

Samples	Atomic concentration (at. %)			
	C	N	O	Ag
Pure GCN	41.1	49.1	9.7	0.0
0.1 AGCN	36.6	56.0	7.3	0.1

**Fig. 5.** UV–VIS absorption spectra for pure GCN and *x*-AGCN samples.

replaced by new cyano bonds (—C=N), represented by a peak at 2173 cm^{-1} , observed for *x*-AGCN samples (Dahiya et al., 2023). Moreover, disturbance peaks appearing at 1232 cm^{-1} , 1313 cm^{-1} , 1397 cm^{-1} , 1453 cm^{-1} , and 1542 cm^{-1} are due to the presence of $\text{sp}^3\text{C—N}$ bonds in the redolent loop structure of GCN (Fan et al., 2017; Paul et al., 2020).

3.4. Surface morphology and compositional analysis

The surfaces morphology of pure GCN sample and 0.1 AGCN sample (representative sample of Ag doped GCN i.e. *x*-AGCN samples) was cross examined by obtaining respective scanning electron microscopy (SEM) images (Fig. 4). It is clear from the SEM image that the surface of pure GCN seems to be irregular, bulky, and comprised of roughly agglomerated layered stacks, whereas for 0.1-AGCN the surface appears in similar nature with smooth, organized, and stratified layers of GCN. Such morphology can be associated to the delamination effect induced by Ag atoms to urea for polymeric condensation and thus restricting the development of bulk layered morphology (Xia et al., 2017; Yu et al., 2014; Zheng et al., 2015). Hence, smooth, fragmented and reasonable porous nature of 0.1 AGCN sample compared to pure GCN can be attributed to the doping effect of Ag into GCN.

The composition analysis of both samples was investigated by energy-dispersive X-ray spectroscopy (EDX), a built-in function of the respective SEM equipment. The atomic concentration for pure GCN and 0.1 AGCN samples is shown in Table 1. The EDX data clearly shows 0.1 AGCN, exhibiting 0.1 atomic % of Ag, which is absent in pure GCN sample, thus distinctly confirming the successful doping of Ag into GCN.

3.5. Optical absorption and band gap estimation

The optical absorption obtained for the pure GCN and *x*-AGCN suspensions is shown in Fig. 5. It is observed that the absorption spectra of all the samples depict the intrinsic absorption of the pure GCN in UV–Visible region with the absorption edge appearing around wavelength of 500 nm (Wudil et al., 2023). Further, the absorption observed

within the visible region ($\lambda = 400\text{--}700\text{ nm}$) for *x*-AGCN samples exhibits redshift, extending absorption towards longer wavelengths upon doping with Ag. It is also noticed that upon increasing the Ag dopant concentration, a humpy peak appears at wavelength of 410 nm for 0.07 AGCN to 0.13 AGCN samples. This peak can be ascribed to the characteristic absorption of Ag nanoparticles due to surface plasmon resonance (SPR) (Karimi-Nazarabad and Goharshadi, 2023), and redshift or extended absorption towards the longer wavelengths for *x*-AGCN samples can be attributed to the creation of defect states within the band gap of GCN, suggesting the doping of Ag atoms into GCN. Moreover, such an absorption peak is not observed for the 0.05 AGCN sample, which might be due to the low concentration of Ag content in it (Barman and Sadhukhan, 2012; Ren et al., 2016).

The band gaps for pure GCN and *x*-AGCN samples were estimated using Tauc's relation (Eq. (1) with consideration of direct band gap ($n = 2$) (Corkill and Cohen, 1993; Dong et al., 2014; Han et al., 2019; Molina and Sansores, 1999; Xu and Gao, 2012). The Tauc's plot for all samples is shown in Fig. 6; the band gap is estimated by extrapolating the linear part of the plot to the zero of x-axis. It is obvious from the estimated band gap values that upon Ag doping, narrowing of the pure GCN band gap occurs. This information firmly suggests the formation of dopant induced energy states within the band gap of pure GCN (Vuggili et al., 2023), leading to enhanced absorption and probably improved photocatalytic performance.

3.6. Photoluminescence (PL) spectroscopy

Photoluminescence (PL) spectroscopy mainly represents electron-hole recombination rate via observing emission spectra obtained as a result of photoexcited charges recombination (Das et al., 2017). The PL spectra for all the samples investigated in the present research work is shown in Fig. 7. It can be seen that the pure GCN sample (Fig. 7a) exhibits a single emission peak centered around 618 nm, whereas Ag doped samples i.e. *x*-AGCN samples display two peaks: 1st peak at 546 nm, and 2nd peak at 715 nm (Wu et al., 2019). It is well established that 2p orbitals of nitrogen create the valence band or the highest occupied molecular orbital (HOMO), while the conduction band or lowest unoccupied molecular orbital (LUMO) is made by sp^2 hybridized carbon–nitrogen group. The excitation of the electrons from the valence band to the conduction band can be ascribed to the 1st peak at 546 nm, whereas the 2nd peak (715 nm) can be ascribed to the emissions caused by recombination of charges trapped at defect states, induced by Ag dopant probably below the conduction band (Das et al., 2017; Wen et al., 2023). As evident from PL spectra of *x*-AGCN samples (Fig. 7b–e), upon Ag doping the 1st peak (546 nm) is quenched significantly, exposing the restricted band to band recombination, by trapping excited electrons at defect states created by Ag dopant, resulting in 2nd emission peak. Moreover, it can also be noticed that with the increase in Ag dopant content, the 2nd peak (715 nm) becomes moderately less from 0.05 AGCN sample to 0.1 AGCN sample, but significantly less for 0.13 AGCN sample. Such dampening, specifically for 0.13 AGCN sample, can be ascribed to heavy doping caused by increased Ag content, letting defect states becoming merely a trapping center. It may also result in decreased photocatalytic performance (Wen et al., 2023). Therefore, it is derived from the above discussion, that the dampening of peaks is caused by the effective doping of Ag into GCN (which is not present in case of pure GCN), making Ag doped sites a suppression center reducing electron-hole recombination. Moreover, the extreme dampening of PL intensity peak for 0.13 AGCN sample (Fig. 7e) is attributed to the increased dopant (Ag) concentration causing surface poisoning by acting as combination sites for electron-hole recombination and limiting the photocatalytic performance (He et al., 2024).

3.7. Photocatalytic performance evaluation

The photocatalytic performance of all the prepared samples i.e., pure

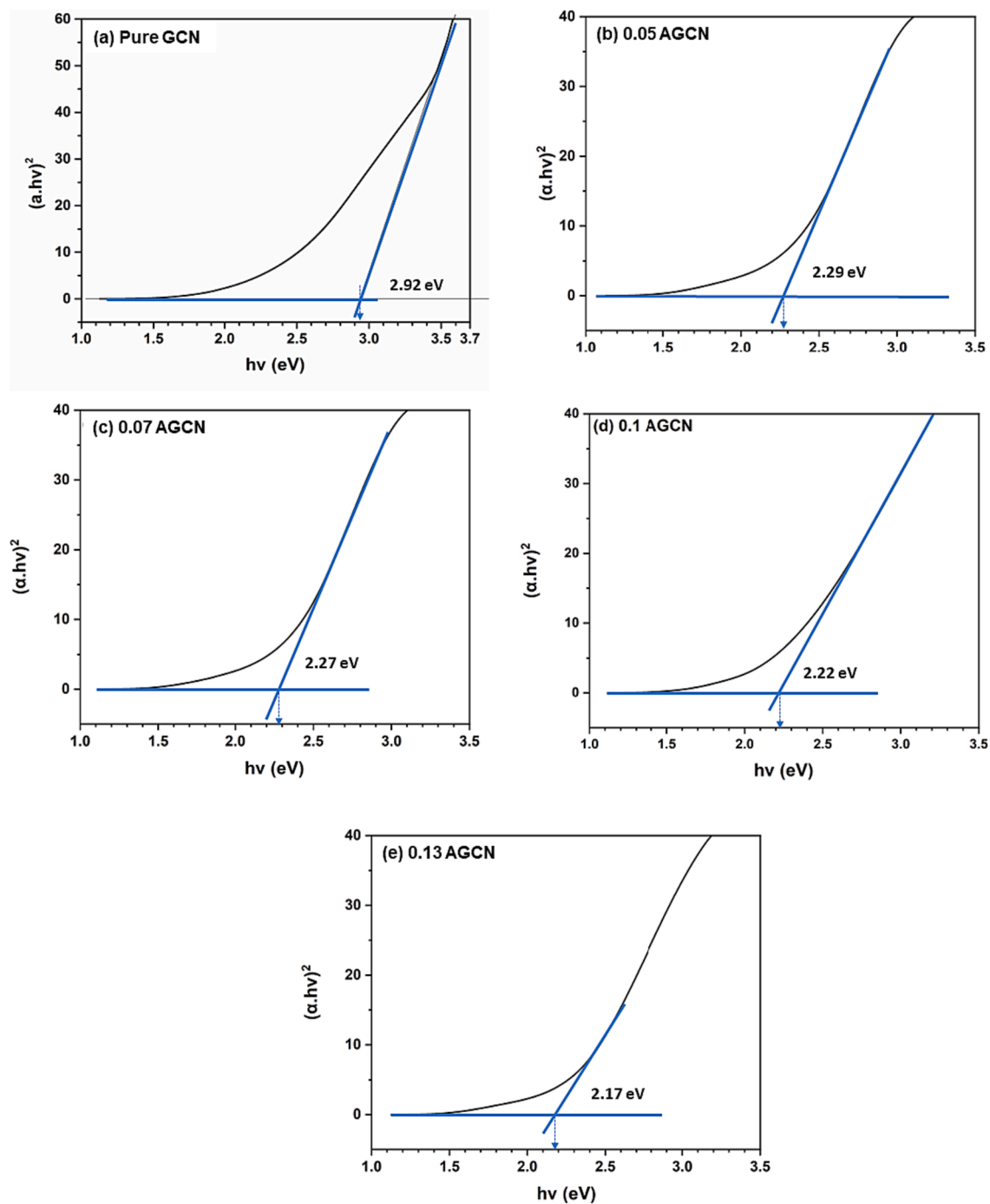


Fig. 6. Estimated band gaps (employing Tauc's relation) for (a) pure GCN, (b) 0.05-AGCN, (c) 0.07-AGCN, (d) 0.1-AGCN, and (e) 0.13 AGCN samples.

GCN and x -AGCN samples, was evaluated by employing them for photodegradation of pharmaceutical pollutant (CIP) under visible light irradiation. Fig. 8 shows the degradation concentration profile and % degradation efficiency (calculated using Eq. (2) for wastewater contaminated with target pollutant i.e. CIP antibiotic. It can be observed that under dark conditions (first 60 min.), there is a decrease in the CIP concentration, ascribed to mere adsorption, intentionally performed to obtain an adsorption-desorption equilibrium curve. However, upon light irradiation, a further decrease in CIP concentration is observed due to photocatalytic degradation reactions occurring at the photocatalyst samples. The maximum change in concentration of CIP (Fig. 8a) and best degradation efficiency (Fig. 8b) is portrayed by 0.1 AGCN sample after 2 h of visible light irradiation, showing degradation efficiency of

approximately 84 %, which is 2.15 times higher than pure GCN samples (39 %). The photocatalytic performance of prepared samples respective to CIP degradation is organized as: 0.1 AGCN > 0.07 AGCN > 0.13 AGCN > 0.05 AGCN > pure GCN. It is interesting to note here that the visible light activity is reducing in the case of 0.13 AGCN because of increasing Ag dopant content, which can be attributed to the fact that recombination centers for photogenerated electron-hole pairs are excessively created and dominantly acting as trapping centers, in turn limiting photocatalytic performance (He et al., 2024). The rate constants (k) for all the samples employing CIP degradation are calculated (using Eq. (3) with consideration of pseudo first order kinetic model and tabulated in Table 2. As noticed, 0.1 AGCN shows the best photocatalytic performance, it shows a rate constant of 0.01 min^{-1} , the maximum

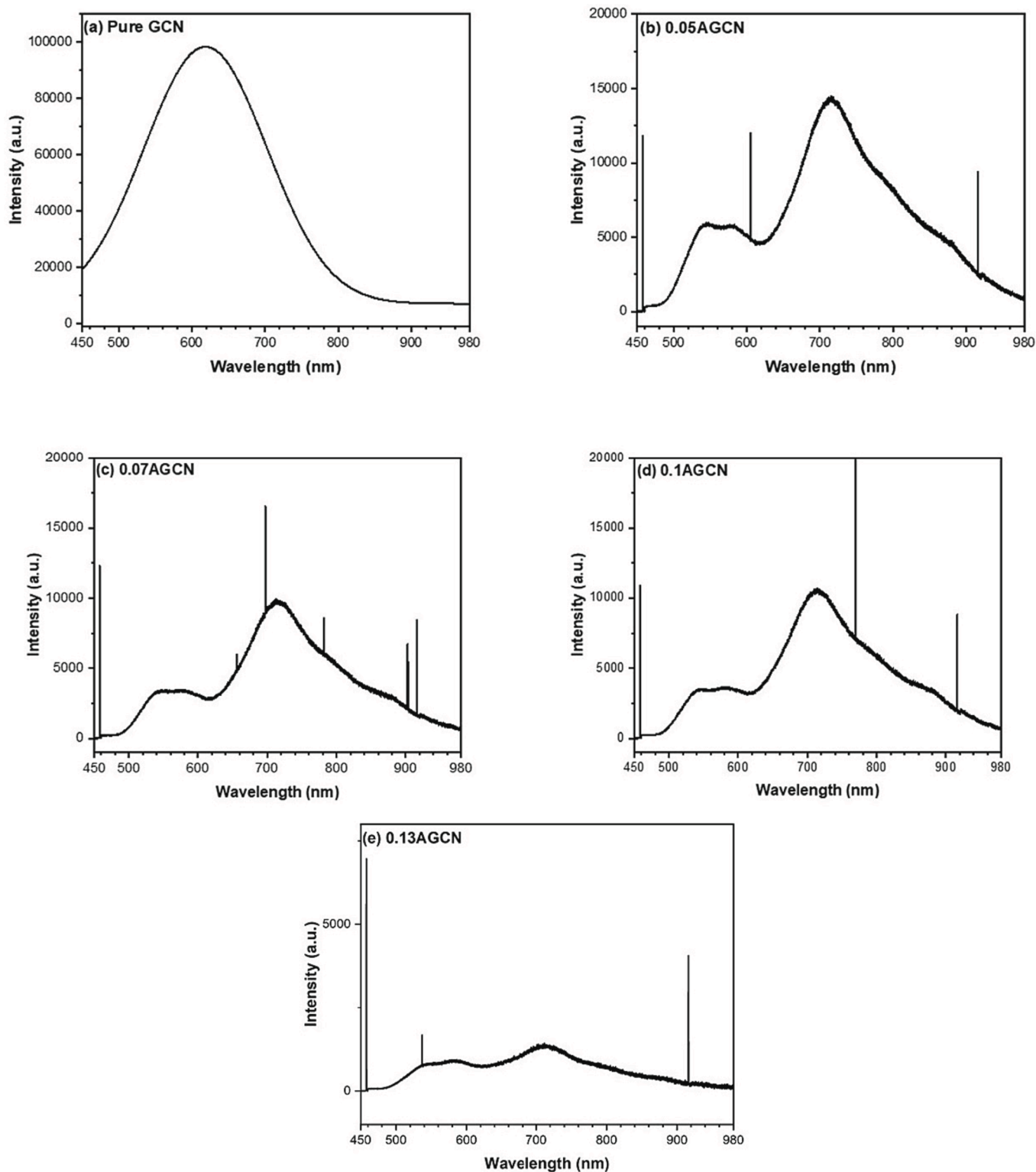


Fig. 7. PL spectra of (a) pure GCN, (b) 0.05 AGCN, (c) 0.07 AGCNs, (d) 0.1 AGCN, and (e) 0.13 AGCN samples.

amongst all the samples.

Increased photocatalytic performance upon Ag doping, can be modestly elucidated on the basis of combined outcome of enhanced light absorption and separation of photogenerated charge carriers (Luo et al., 2021). It is obvious, upon Ag doping the light absorption edge of pure GCN is shifted towards the red region and extended light absorption depicting the creation of defect states leading to band gap narrowing (Das et al., 2020). Such defects states within the band gap and narrowing

of the band gap, resulting in enhanced light absorption will lead to increased photogenerated charges (e^-h^+ pairs) (Tahir et al., 2022). Concurrently, the PL spectra show quenching of band-to-band excitation peak (1st peak at 546 nm), enlightening the efficient separation of photogenerated charges, which are likely to be trapped at the defect levels, followed by their diffusion to photocatalysts surface to degrade CIP ultimately. Further when the Ag dopant concentration is increased in samples from 0.05 AGCN to 0.1 AGCN sample, improvement in

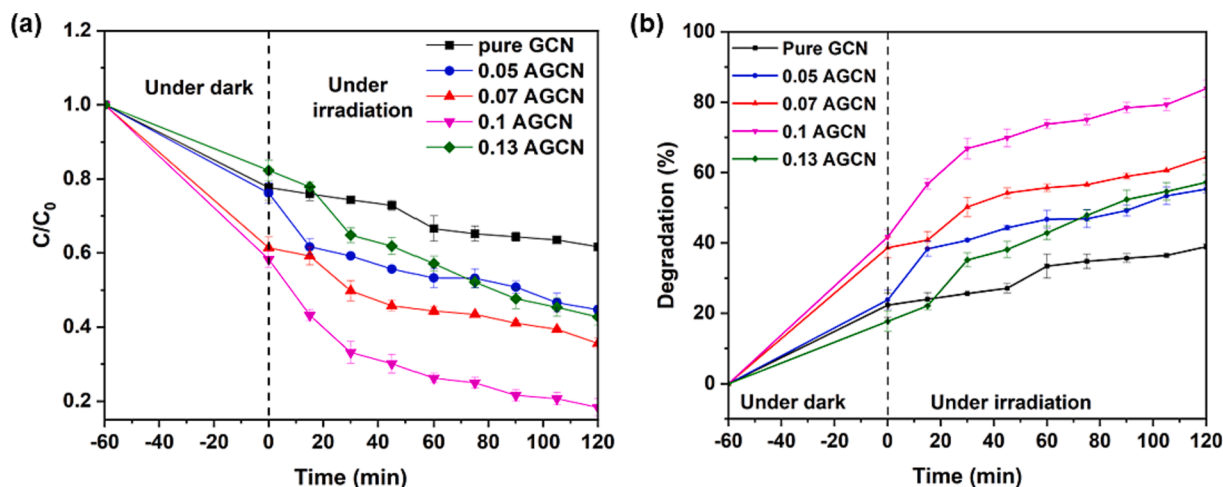


Fig. 8. Photocatalytic performance evaluation of pure GCN and x -AGCN samples demonstrated by (a) change in concentration and (b) degradation efficiency of simulated CIP wastewater.

Table 2

Rate constants calculated for all samples with consideration of pseudo first kinetic model.

Sample name	Rate constant, k (min^{-1})
Pure GCN	0.00259563
0.05-AGCN	0.004512549
0.07-AGCN	0.00530978
0.1-AGCN	0.010147777
0.13-AGCN	0.005390168

photocatalytic performance is observed. However, upon increasing the Ag dopant amount i.e., in sample 0.13 AGCN, a decrease in the photocatalytic activity is noticed. The reason for such a decrease can be explained by PL spectra, which depicts a decrease in the emission intensity of defect induced peak (2nd peak at 715 nm), indicating the trapping of photogenerated electrons for a prolonged duration (Li et al., 2022; Liu et al., 2020). Hence it can be stipulated that there exists an optimum value of Ag dopant well balancing the light absorption and charge separation, resulting in the enhanced photocatalytic performance of Ag doped GCN, evaluated by CIP degradation.

The photocatalytic degradation mechanism for CIP contaminated water is well established in literature based on experimental findings and investigations (Ao et al., 2018; Guo et al., 2022a; Nie et al., 2022; Noroozi et al., 2022; Pan et al., 2022; Sayed et al., 2016; Wang et al., 2021). Recently, research work done by (Chen et al., 2024), demonstrates the photocatalytic conversion of CIP into several intermediate species and identified using LC-MS, which undergoes series of reactions

finally mineralizing into H_2O and CO_2 . The degradation pathway reported involves the adsorbed species attacked by $\text{O}_2^{\bullet-}$ and OH^{\bullet} forming reactive intermediate species which undergoes series of reaction and at the later stage are mineralized to H_2O and CO_2 (Chen et al., 2024).

A similar degradation mechanism is proposed in the present study, displayed by Fig. 9 and Eqs. (4)–(10). It can be interpreted that Ag doping improves optical absorption and charge separation, leading to enhanced photogenerated charges and separation. The photogenerated electrons in the conduction band and at defect states can reduce O_2 to $\text{O}_2^{\bullet-}$, whereas holes in the valence band can oxidize OH^- to OH^{\bullet} . Both species can react with CIP adsorbed on the surface or in solution to several intermediate reactive species which ultimately results in the degradation products. Hence based on well reports and established literature, various reactions presumed to be involved in the CIP degradation are shown in Eqs. (4)–(10) (Li et al., 2020; Salma et al., 2016).

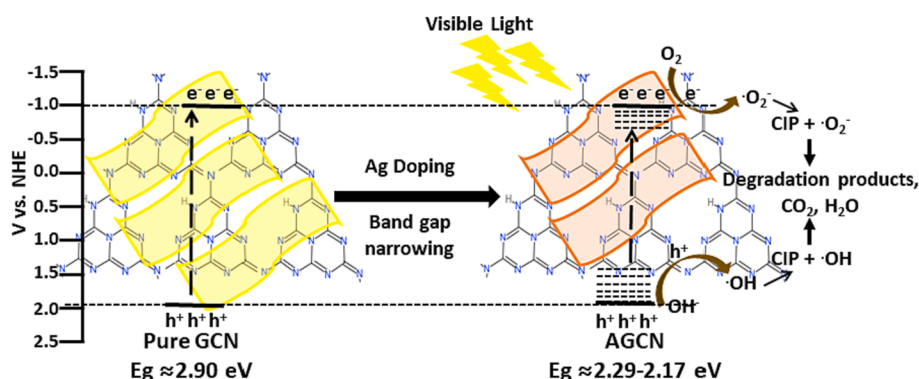


Fig. 9. Proposed mechanism for the photocatalytic degradation of CIP polluted wastewater.

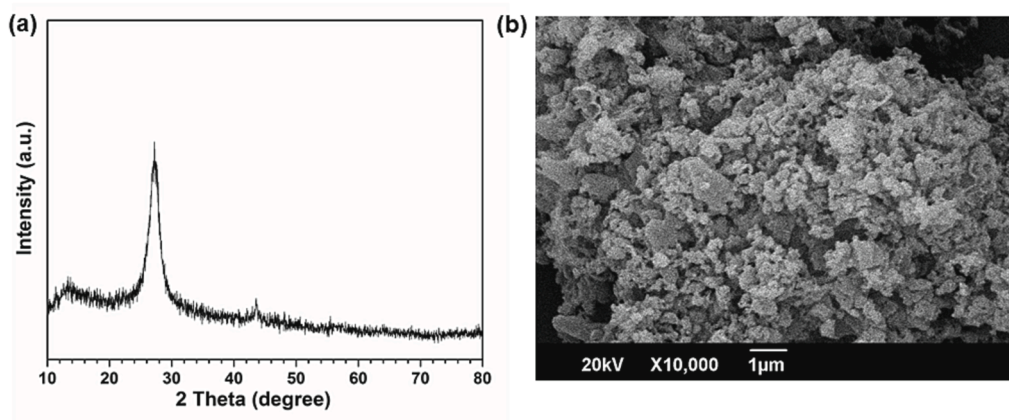


Fig. 10. (a) XRD pattern, and (b) SEM image of 0.1 AGCN spent sample after employed for CIP degradation.

Table 3
Comparison of different photocatalysts employed for CIP degradation.

Photocatalyst	Light source	CIP degradation efficiency	Reference
Ag doped GCN (x-AGCN)	5 W, white LED light	84 %	Present work
In ₂ O ₃ /BiOBr	300 W, Xenon lamp (CEL – LAM300) with 420 nm cutoff filter	93.5 %	(Cheng et al., 2024)
Bi/BiOCOOH/PVDF composite	150 W, High-pressure sodium lamps (HPSL)	89 %	(Shen et al., 2023)
Platinum anchored thiophene ring doped carbon nitride nanosheets, (Pt _{1.0} -CAN)	300 W, Xenon lamp with a 400 nm cutoff filter	44.4%	(Wu et al., 2023)
Ce(MoO ₄) ₂ /g-C ₃ N ₄ composite	35 W, Xe arc lamp used with color temperature of 6000 K	78.1 %	(Gandamalla et al., 2024)
Titanium carbide MXene reinforced g-C ₃ N ₄ , Ti ₃ C ₂ (MX/CN)	300 W, Xenon lamp with λ > 400 nm	97.98 %	(Zhang et al., 2024)



Fig. 10 displays the XRD and SEM image of the spent 0.1 AGCN sample (optimum Ag doped GCN showing best degradation performance) after being employed for CIP degradation. It can be observed that both XRD and SEM don't show any major changes thus suggesting the Ag doped sample to be quite stable during the photocatalytic reactions and process.

Table 3 shows summarized comparison of different photocatalysts reported in literature, employed for CIP degradation. The photocatalytic material, light irradiation source and degradation (%) are compared with respect to photocatalytic CIP degradation. It can be realized from the table that optimum Ag doped GCN sample (0.1 AGCN), synthesized in the present work exhibits better performance, most importantly under visible light irradiation from a 5 W light source as compared to other mentioned research works employing high energy light sources (Phoon et al., 2020).

4. Conclusions

Ag doped GCN photocatalysts were synthesized successfully employing a facile and simple synthesis approach executing the aim of

visible light active photocatalyst. The photocatalytic performance of pure GCN and Ag doped GCN (x-AGCN), with varied content of Ag dopant, was evaluated concerning the degradation of CIP, a prominent antibiotic micropollutant whose use had also been increased during and post COVID-19 pandemic. In particular, the photocatalytic CIP degradation was evaluated under 5 W LED light irradiation. The sample with optimum content of Ag, i.e. 0.1 AGCN sample showed maximal photocatalytic performance, thus acting as the best sample. The improved photocatalytic performance upon Ag doping can be ascribed to the collaborative effect of improved optical absorption and modest photo-generated charge separation, with increased Ag dopant content to a maximum performance and then decreased. The improved optical absorption is ascribed to band gap narrowing induced by defect states, whereas the quenching of emission spectra is associated to the trapping of band-to-band photoexcited charges by defect states. Upon further increasing Ag dopant content, above optimum level, the photocatalytic performance is decreased and is ascribed to excessive doping forming immoderate defects acting as merely recombination centers for photo-excited electron-hole pairs. Conclusively, a simple synthesis strategy of Ag-doped GCN is suggested with the objectives of eco-friendly, visible light active, narrow band gap photocatalyst through cost effective doping of pure-GCN providing favorable results in the present experimental work. It is expected this research will pave the way forward for the development of visible light active photocatalysts with high efficiencies towards PMP removal in the domain of AOP and photocatalytic wastewater treatment.

Declaration of Competing Interest

The authors declare that they have no known competing financial interests or personal relationships that could have appeared to influence the work reported in this paper.

Acknowledgements

This work was supported by The Higher Education Commission (HEC), Pakistan under the Startup Research Grant for Fresh PhD Holders, Project No. 21-1952/SRGP/R&D/HEC/2018, a National University Development Project funded by the Ministry of Education (Korea) and the National Research Foundation of Korea (2022).

References

- Abromaitis, V., Svaikauskaitė, J., Sulciute, A., Sinkeviciute, D., Zmuidzinaviciene, N., Misevicius, S., Tichonovas, M., Urniezaitė, I., Jankunaite, D., Urbonavicius, M., Varnagiris, S., Dzingeleviciene, R., Baranauskis, K., Martuzevicius, D., 2022. Ozone-enhanced TiO₂ nanotube arrays for the removal of COVID-19 aided antibiotic

- ciprofloxacin from water: process implications and toxicological evaluation. *J. Environ. Manage.* 318, 115515 <https://doi.org/10.1016/j.jenvman.2022.115515>.
- An, T., Yang, H., Li, G., Song, W., Cooper, W.J., Nie, X., 2010. Kinetics and mechanism of advanced oxidation processes (AOPs) in degradation of ciprofloxacin in water. *Appl. Catal. B* 94, 288–294. <https://doi.org/10.1016/j.apcatb.2009.12.002>.
- Ao, X., Liu, W., Sun, W., Cai, M., Ye, Z., Yang, C., Lu, Z., Li, C., 2018. Medium pressure UV-activated peroxymonosulfate for ciprofloxacin degradation: kinetics, mechanism, and genotoxicity. *Chem. Eng. J.* 345, 87–97. <https://doi.org/10.1016/j.cej.2018.03.133>.
- Aruljothi, C., Balaji, P., Vaishnavi, E., Pazhanivel, T., Vasuki, T., 2023. Magnetic recyclable CuFe₂O₄/rGO nanocomposite for the degradation of tetracycline under sunlight irradiation. *J. Chem. Technol. Biotechnol.* 98, 1908–1917. <https://doi.org/10.1002/jctb.7408>.
- Ashfaq, M., Li, Y., Rehman, M.S.U., Zubair, M., Mustafa, G., Nazar, M.F., Yu, C.P., Sun, Q., 2019. Occurrence, spatial variation and risk assessment of pharmaceuticals and personal care products in urban wastewater, canal surface water, and their sediments: a case study of Lahore, Pakistan. *Sci. Total Environ.* 688, 653–663. <https://doi.org/10.1016/j.scitotenv.2019.06.285>.
- Bahnemann, D., 2004. Photocatalytic water treatment: solar energy applications. *Sol. Energy* 77, 445–459. <https://doi.org/10.1016/j.solener.2004.03.031>.
- Bai, X., Zong, R., Li, C., Liu, D., Liu, Y., Zhu, Y., 2014. Enhancement of visible photocatalytic activity via Ag@C₃N₄ core-shell plasmonic composite. *Appl. Catal. B* 147, 82–91. <https://doi.org/10.1016/j.apcatb.2013.08.007>.
- Barman, S., Sadhukhan, M., 2012. Facile bulk production of highly blue fluorescent graphitic carbon nitride quantum dots and their application as highly selective and sensitive sensors for the detection of mercuric and iodide ions in aqueous media. *J. Mater. Chem.* 22, 21832–21837. <https://doi.org/10.1039/c2jm35501a>.
- Belhaj, D., Baccar, R., Jaabiri, I., Bouzid, J., Kallel, M., Ayadi, H., Zhou, J.L., 2015. Fate of selected estrogenic hormones in an urban sewage treatment plant in Tunisia (North Africa). *Sci. Total Environ.* 505, 154–160. <https://doi.org/10.1016/j.scitotenv.2014.10.018>.
- Bera, S.P., Godhaniya, M., Kothari, C., 2022. Emerging and advanced membrane technology for wastewater treatment: a review. *J. Basic Microbiol.* 62, 245–259. <https://doi.org/10.1002/jobm.202100259>.
- Bhuvanewari, K., Palanisamy, G., Pazhanivel, T., Maiyalagan, T., Shanmugam, P., Grace, A.N., 2021. In-situ development of metal organic frameworks assisted ZnMgAl layered triple hydroxide 2D/2D hybrid as an efficient photocatalyst for organic dye degradation. *Chemosphere* 270, 128616. <https://doi.org/10.1016/j.chemosphere.2020.128616>.
- Bhuvanewari, K., Sreeja, B.S., Radha, S., Saranya, J., Palanisamy, G., Srinivasan, M., Pazhanivel, T., 2023. Facile assembly of effective carbon quantum dots and multiwall carbon nanotubes supported MnO₂ hybrid nanoparticles for enhanced photocatalytic and anticancer activity. *Inorg. Chem. Commun.* 148, 110250 <https://doi.org/10.1016/j.inoche.2022.110250>.
- Bojdys, M.J., Müller, J.O., Antonietti, M., Thomas, A., 2008. Ionothermal synthesis of crystalline, condensed, graphitic carbon nitride. *Chem. A Eur. J.* 14, 8177–8182. <https://doi.org/10.1002/chem.200800190>.
- Bu, Y., Chen, Z., Li, W., 2014. Using electrochemical methods to study the promotion mechanism of the photoelectric conversion performance of Ag-modified mesoporous g-C₃N₄ heterojunction material. *Appl. Catal. B* 144, 622–630. <https://doi.org/10.1016/j.apcatb.2013.07.066>.
- Chakrabarti, S., Dutta, B.K., 2004. Photocatalytic degradation of model textile dyes in wastewater using ZnO as semiconductor catalyst. *J. Hazard. Mater.* 112, 269–278. <https://doi.org/10.1016/j.jhazmat.2004.05.013>.
- Chander, V., Sharma, B., Negi, V., Aswal, R.S., Singh, P., Singh, R., Dobhal, R., 2016. Pharmaceutical compounds in drinking water. *J. Xenobiot* 6, 1–7. <https://doi.org/10.4081/xeno.2016.5774>.
- Chen, X., Lei, L., Liu, S., Han, J., Li, R., Men, J., Li, L., Wei, L., Sheng, Y., Yang, L., Zhou, B., Zhu, L., 2021. Occurrence and risk assessment of pharmaceuticals and personal care products (PPCPs) against COVID-19 in lakes and WWTP-river-estuary system in Wuhan, China. *Sci. Total Environ.* 792, 148352 <https://doi.org/10.1016/j.scitotenv.2021.148352>.
- Chen, M., Yang, T., Zhao, L., Shi, X., Li, R., Ma, L., Huang, Y., Wang, Y., Lee, S., Cheng, 2024. Manganese oxide on activated carbon with peroxymonosulfate activation for enhanced ciprofloxacin degradation: activation mechanism and degradation pathway. *Appl. Surf. Sci.* 645, 158835 <https://doi.org/10.1016/j.apsusc.2023.158835>.
- Cheng, J., Deng, Z., Zheng, X., Chu, C., Guo, Y., 2024. Construction and actual application of In₂O₃/BiOBr heterojunction for effective removal of ciprofloxacin under visible light: photocatalytic mechanism, DFT calculation, degradation pathway and toxicity evaluation. *J. Alloy. Compd.* 971, 172779 <https://doi.org/10.1016/j.jallcom.2023.172779>.
- Conceicao, K.C., Villamar-Ayala, C.A., Plaza-Garrido, A., Toledo-Neira, C., 2023. Seasonal behavior of pharmaceuticals and personal care products within Chilean rural WWTPs under COVID-19 pandemic conditions. *J. Environ. Chem. Eng.* 11, 110984 <https://doi.org/10.1016/j.jece.2023.110984>.
- Corkill, J.L., Cohen, M.L., 1993. Calculated quasiparticle band gap of g-C₃N₄. *Phys. Rev. B* 48, 17622–17624. <https://doi.org/10.1103/PhysRevB.48.17622>.
- Dahiya, S., Sharma, A., Chaudhary, S., 2023. Synthesis of phytoextract-mediated Ag-doped graphitic carbon nitride (Ag@GCN) for photocatalytic degradation of dyes. *Environ. Sci. Pollut. Res.* 30, 25650–25662. <https://doi.org/10.1007/s11356-023-25359-0>.
- Das, D., Banerjee, D., Pahari, D., Ghorai, U.K., Sarkar, S., Das, N.S., Chattopadhyay, K.K., 2017. Defect induced tuning of photoluminescence property in graphitic carbon nitride nanosheets through synthesis conditions. *J. Lumin.* 185, 155–165. <https://doi.org/10.1016/j.jlumin.2017.01.007>.
- Das, D., Banerjee, D., Mondal, M., Shett, A., Das, B., Das, N.S., Ghorai, U.K., Chattopadhyay, K.K., 2018. Nickel doped graphitic carbon nitride nanosheets and its application for dye degradation by chemical catalysis. *Mater. Res. Bull.* 101, 291–304. <https://doi.org/10.1016/j.materresbull.2018.02.004>.
- Das, R.S., Warkhade, S.K., Kumar, A., Gaikwad, G.S., Wankhade, A.V., 2020. Graphitic carbon nitride @ silver zirconate nanocomposite (gC₃N₄@Ag₂ZrO₃): a Type-II heterojunction for an effective visible light photocatalysis and bacterial photo-inactivation. *J. Alloy. Compd.* 846, 155770 <https://doi.org/10.1016/j.jallcom.2020.155770>.
- de Ilurdoz, M.S., Sadhwani, J.J., Reboso, J.V., 2022. Antibiotic removal processes from water & wastewater for the protection of the aquatic environment - a review. *J. Water Process Eng.* 45, 102474 <https://doi.org/10.1016/j.jwpe.2021.102474>.
- Demir, M., Gökçug, T.H., Bulut, Y., 2014. Human-induced water pollution and management. *Fresenius Environ. Bull.* 23, 478–488.
- Dong, G., Zhang, Y., Pan, Q., Qiu, J., 2014. A fantastic graphitic carbon nitride (g-C₃N₄) material: electronic structure, photocatalytic and photoelectronic properties. *J. Photochem. Photobiol. C: Photochem. Rev.* 20, 33–50. <https://doi.org/10.1016/j.jphotochemrev.2014.04.002>.
- Du, A., Sanvito, S., Li, Z., Wang, D., Jiao, Y., Liao, T., Sun, Q., Ng, Y.H., Zhu, Z., Amal, R., Smith, S.C., 2012. Hybrid graphene and graphitic carbon nitride nanocomposite: gap opening, electron-hole puddle, interfacial charge transfer, and enhanced visible light response. *J. Am. Chem. Soc.* 134, 4393–4397. <https://doi.org/10.1021/ja211637p>.
- Eniola, J.O., Kumar, R., Barakat, M.A., Rashid, J., 2022. A review on conventional and advanced hybrid technologies for pharmaceutical wastewater treatment. *J. Clean. Prod.* 356, 131826 <https://doi.org/10.1016/j.jclepro.2022.131826>.
- Fan, Q., Liu, J., Yu, Y., Zuo, S., Li, B., 2017. A simple fabrication for sulfur doped graphitic carbon nitride porous rods with excellent photocatalytic activity degrading RhB dye. *Appl. Surf. Sci.* 391, 360–368. <https://doi.org/10.1016/j.apsusc.2016.04.055>.
- Gandamalla, A., Manchala, S., Verma, A., Fu, Y.P., Shanker, V., 2024. Development of highly efficient Ce(MoO₄)₂/g-C₃N₄ composite for the photocatalytic degradation of methylene blue and ciprofloxacin under visible light. *J. Mol. Struct.* 1297, 136896 <https://doi.org/10.1016/j.molstruc.2023.136896>.
- Ge, L., Han, C., Liu, J., 2011. Novel visible light-induced g-C₃N₄/Bi₂WO₆ composite photocatalysts for efficient degradation of methyl orange. *Appl. Catal. B* 108–109, 100–107. <https://doi.org/10.1016/j.apcatb.2011.08.014>.
- Ghazal, H., Koumaki, E., Hoslett, J., Malamis, S., Katsou, E., Barcelo, D., Jouhara, H., 2022. Insights into current physical, chemical and hybrid technologies used for the treatment of wastewater contaminated with pharmaceuticals. *J. Clean. Prod.* 361, 132079 <https://doi.org/10.1016/j.jclepro.2022.132079>.
- Guo, X., Duan, J., Wang, W., Zhang, Z., 2020. Modified graphitic carbon nitride as the photocatalyst for wastewater treatment under visible light irradiation. *Fuel* 280, 118544. <https://doi.org/10.1016/j.fuel.2020.118544>.
- Guo, Q., Peng, Y., Chao, K., 2022b. Raman enhancement effect of different silver nanoparticles on salbutamol. *Heliyon* 8, e09576.
- Guo, Y., Wang, R., Wang, P., Li, Y., Wang, C., 2017. Developing polyetherimide/graphitic carbon nitride floating photocatalyst with good photodegradation performance of methyl orange under light irradiation. *Chemosphere* 179, 84–91. <https://doi.org/10.1016/j.chemosphere.2017.03.085>.
- Guo, F., Zhang, H., Li, H., Shen, Z., 2022a. Modulating the oxidative active species by regulating the valence of palladium cocatalyst in photocatalytic degradation of ciprofloxacin. *Appl. Catal. B* 306, 121092. <https://doi.org/10.1016/j.apcatb.2022.121092>.
- Han, C., Ge, L., Chen, C., Li, Y., Zhao, Z., Xiao, X., Li, Z., Zhang, J., 2014. Site-selected synthesis of novel Ag@AgCl nanoframes with efficient visible light induced photocatalytic activity. *J. Mater. Chem. A Mater.* 2, 12594–12600. <https://doi.org/10.1039/c4ta01941e>.
- Han, S., Hu, X., Yang, W., Qian, Q., Fang, X., Zhu, Y., 2019. Constructing the band alignment of graphitic carbon nitride (g-C₃N₄)/Copper(I) oxide (Cu₂O) composites by adjusting the contact facet for superior photocatalytic activity. *ACS Appl. Energy Mater.* 2, 1803–1811. <https://doi.org/10.1021/acsami.8b01930>.
- He, Y., Xia, J., Ye, J., Tong, Y., Chen, X., He, G., Chen, H., 2024. Materials Science in Semiconductor Processing Design of Co-doped carbon nitride based on melem supramolecular assembly with enhanced photocatalytic activity toward tetracycline hydrochloride degradation. *Mater. Sci. Semicond. Process.* 171, 107999 <https://doi.org/10.1016/j.mssp.2023.107999>.
- Hu, S.W., Yang, L.W., Tian, Y., Wei, X.L., Ding, J.W., Zhong, J.X., Chu, P.K., 2015. Simultaneous nanostructure and heterojunction engineering of graphitic carbon nitride via in situ Ag doping for enhanced photoelectrochemical activity. *Appl. Catal. B* 163, 611–622. <https://doi.org/10.1016/j.apcatb.2014.08.023>.
- Jiang, L., Yuan, X., Pan, Y., Liang, J., Zeng, G., Wu, Z., Wang, H., 2017. Doping of graphitic carbon nitride for photocatalysis: a review. *Appl. Catal. B* 217, 388–406. <https://doi.org/10.1016/j.apcatb.2017.06.003>.
- Jiang, J., Zou, J., Wee, A.T.S., Zhang, W., 2016. Use of single-layer g-C₃N₄/Ag hybrids for surface-enhanced raman scattering (SERS). *Sci. Rep.* 6, 1–10. <https://doi.org/10.1038/srep34599>.
- Karimi-Nazarabad, M., Goharshadi, E.K., 2023. Ag and Ni doped graphitic carbon nitride coated on wood as a highly porous and efficient photoabsorber in interfacial solar steam generation. *J. Porous Mater.* 1–8 <https://doi.org/10.1007/s10934-023-01468-6>.
- Khan, K., Kar, S., Roy, K., 2023. Are we ready to combat the ecotoxicity of COVID-19 pharmaceuticals? An in silico aquatic risk assessment. *Aquat. Toxicol.* 256, 106416 <https://doi.org/10.1016/j.aquatox.2023.106416>.
- Kora, A.J., Arunachalam, J., 2012. Green fabrication of silver nanoparticles by gum tragacanth (astragalus gummifer): a dual functional reductant and stabilizer. *J. Nanomater.* 2012 <https://doi.org/10.1155/2012/869765>.

- Krýsa, J., Bouzek, K., Stollberg, C., 2000. Photocatalytic degradation of oxalic acid on a semiconductive layer of n-TiO₂ particles in a batch plate reactor. Part III: rate determining steps and nonsteady diffusion model for oxygen transport. *J. Appl. Electrochem.* 30, 1033–1041. <https://doi.org/10.1023/A:1004082301593>.
- Kudin, K.N., Ozbas, B., Schniepp, H.C., Prud'homme, R.K., Aksay, I.A., Car, R., 2008. Raman spectra of graphite oxide and functionalized graphene sheets. *Nano Lett* 8, 36–41. <https://doi.org/10.1021/nl071822y>.
- Kumar, A., Raizada, P., Singh, P., Saini, R.V., Saini, A.K., Hosseini-Bandegharai, A., 2020. Perspective and status of polymeric graphitic carbon nitride based Z-scheme photocatalytic systems for sustainable photocatalytic water purification. *Chem. Eng. J.* 391, 123496. <https://doi.org/10.1016/j.cej.2019.123496>.
- Kümmerer, K., 2009. The presence of pharmaceuticals in the environment due to human use - present knowledge and future challenges. *J. Environ. Manage.* 90, 2354–2366. <https://doi.org/10.1016/j.jenvman.2009.01.023>.
- Lakatos, G., 2018. Biological wastewater treatment. *Wastewater and Water Contamination: Sources, Assessment and Remediation* 105–128. doi: 10.1201/b18368-4.
- Lee, K.M., Lai, C.W., Ngai, K.S., Juan, J.C., 2016. Recent developments of zinc oxide based photocatalyst in water treatment technology: a review. *Water Res.* 88, 428–448. <https://doi.org/10.1016/j.watres.2015.09.045>.
- Lee, S.Y., Park, S.J., 2013. TiO₂ photocatalyst for water treatment applications. *J. Ind. Eng. Chem.* 19, 1761–1769. <https://doi.org/10.1016/j.jiec.2013.07.012>.
- Li, S., Huang, T., Du, P., Liu, W., Hu, J., 2020. Photocatalytic transformation fate and toxicity of ciprofloxacin related to dissociation species: experimental and theoretical evidences. *Water Res.* 185. <https://doi.org/10.1016/j.watres.2020.116286>.
- Li, H., Jing, Y., Ma, X., Liu, T., Yang, L., Liu, B., Yin, S., Wei, Y., Wang, Y., 2017. Construction of a well-dispersed Ag/graphene-like g-C₃N₄ photocatalyst and enhanced visible light photocatalytic activity. *RSC Adv.* 7, 8688–8693. <https://doi.org/10.1039/c6ra26498k>.
- Li, D., Shi, W., 2016. Recent developments in visible-light photocatalytic degradation of antibiotics. *Cuihua Xuebao/Chin. J. Catal.* 37, 792–799. [https://doi.org/10.1016/S1872-2067\(15\)61054-3](https://doi.org/10.1016/S1872-2067(15)61054-3).
- Li, W., Wei, Z., Zhu, K., Wei, W., Yang, J., Jing, J., Phillips, D.L., Zhu, Y., 2022. Nitrogen-defect induced trap states steering electron-hole migration in graphite carbon nitride. *Appl. Catal. B* 306, 121142. <https://doi.org/10.1016/j.apcatb.2022.121142>.
- Li, X., Zhang, J., Shen, L., Ma, Y., Lei, W., Cui, Q., Zou, G., 2009. Preparation and characterization of graphitic carbon nitride through pyrolysis of melamine. *Appl. Phys. A Mater. Sci. Process.* 94, 387–392. <https://doi.org/10.1007/s00339-008-4816-4>.
- Liu, H., Ma, S., Shao, L., Liu, H., Gao, Q., Li, B., Fu, H., Fu, S., Ye, H., Zhao, F., Zhou, J., 2020. Defective engineering in graphitic carbon nitride nanosheet for efficient photocatalytic pathogenic bacteria disinfection. *Appl. Catal. B* 261, 118201. <https://doi.org/10.1016/j.apcatb.2019.118201>.
- Liu, W., Wang, M., Xu, C., Chen, S., 2012. Facile synthesis of g-C₃N₄/ZnO composite with enhanced visible light photooxidation and photoreduction properties. *Chem. Eng. J.* 209, 386–393. <https://doi.org/10.1016/j.cej.2012.08.033>.
- Liu, X.R., Zinin, P.V., Ming, L.C., Acosta, T., Sharma, S.K., Misra, A.K., Hong, S.M., 2010. Raman spectroscopy of melamine at high pressures. *J. Phys. Conf. Ser.* 215. <https://doi.org/10.1088/1742-6596/215/1/012045>.
- Luo, T., Hu, X., She, Z., Wei, J., Feng, X., Chang, F., 2021. Synergistic effects of Ag-doped and morphology regulation of graphitic carbon nitride nanosheets for enhanced photocatalytic performance. *J. Mol. Liq.* 324, 114772. <https://doi.org/10.1016/j.molliq.2020.114772>.
- Luo, L., Zhang, A., Janik, M.J., Li, K., Song, C., Guo, X., 2017. Facile fabrication of ordered mesoporous graphitic carbon nitride for RhB photocatalytic degradation. *Appl. Surf. Sci.* 396, 78–84. <https://doi.org/10.1016/j.apsusc.2016.10.190>.
- Molina, B., Sansores, L.E., 1999. Electronic structure of six phases of C₃N₄. A theoretical approach. *Mod. Phys. Lett. B* 13, 193–201. <https://doi.org/10.1142/s0217984999000269>.
- Nie, X., Li, G., Li, S., Luo, Y., Luo, W., Wan, Q., An, T., 2022. Highly efficient adsorption and catalytic degradation of ciprofloxacin by a novel heterogeneous Fenton catalyst of hexapod-like pyrite nanosheets mineral clusters. *Appl. Catal. B* 300, 120734. <https://doi.org/10.1016/j.apcatb.2021.120734>.
- Noroozi, R., Gholami, M., Farzadkia, M., Jonidi Jafari, A., 2022. Degradation of ciprofloxacin by CuFe₂O₄/GO activated PMS process in aqueous solution: performance, mechanism and degradation pathway. *Int. J. Environ. Anal. Chem.* 102, 174–195. <https://doi.org/10.1080/03067319.2020.1718669>.
- Pan, Y., Hu, X., Shen, D., Li, Z., Chen, R., Li, Y., Lu, J., Bao, M., 2022. Facile construction of Z-scheme Fe-MOF@BiOBr/M-CN heterojunction for efficient degradation of ciprofloxacin. *Sep. Purif. Technol.* 295, 121216. <https://doi.org/10.1016/j.seppur.2022.121216>.
- Parasuraman, B., Kandasamy, B., Murugan, I., Alsalmi, M.S., Asemi, N., Thangavelu, P., Perumal, S., 2023a. Designing the heterostructured FeWO₄/FeS₂ nanocomposites for an enhanced photocatalytic organic dye degradation. *Chemosphere* 334, 1–9. <https://doi.org/10.1016/j.chemosphere.2023.138979>.
- Parasuraman, B., Vasudevan, V., Kandasamy, B., Rangaraju, H., Thangavelu, P., 2023b. Development of Bi₂S₃/Cu₂S heterojunction as an effective photocatalysts for the efficient degradation of antibiotic drug and organic dye. *Environ. Sci. Pollut. Res.* 1–12. <https://doi.org/10.1007/s11356-023-26627-9>.
- Paul, D.R., Sharma, R., Panchal, P., Nehra, S.P., Gupta, A.P., Sharma, A., 2020. Synthesis, characterization and application of silver doped graphitic carbon nitride as photocatalyst towards visible light photocatalytic hydrogen evolution. *Int. J. Hydrogen Energy* 45, 23937–23946. <https://doi.org/10.1016/j.ijhydene.2019.06.061>.
- Pawar, R.C., Kang, S., Ahn, S.H., Lee, C.S., 2015. Gold nanoparticle modified graphitic carbon nitride/multi-walled carbon nanotube (g-C₃N₄/CNTs/Au) hybrid photocatalysts for effective water splitting and degradation. *RSC Adv.* 5, 24281–24292. <https://doi.org/10.1039/c4ra15560b>.
- Pham, T.H., Jung, S.H., Kim, T.Y., 2021. Enhanced photodegradation of toxic volatile organic pollutants using Ni-doped graphitic carbon nitride under natural solar light. *Sol. Energy* 224, 18–26. <https://doi.org/10.1016/j.solener.2021.05.087>.
- Pham, T.H., Myung, Y., Van Le, Q., Kim, T., 2022. Visible-light photocatalysis of Ag-doped graphitic carbon nitride for photodegradation of micropollutants in wastewater. *Chemosphere* 301, 134626. <https://doi.org/10.1016/j.chemosphere.2022.134626>.
- Phoon, B.L., Ong, C.C., Mohamed Saheed, M.S., Show, P.L., Chang, J.S., Ling, T.C., Lam, S.S., Juan, J.C., 2020. Conventional and emerging technologies for removal of antibiotics from wastewater. *J. Hazard. Mater.* 400, 122961. <https://doi.org/10.1016/j.jhazmat.2020.122961>.
- Prabakaran, E., Pillay, K., 2021. Self-assembled silver nanoparticles decorated on exfoliated graphitic carbon nitride/carbon sphere nanocomposites as a novel catalyst for catalytic reduction of Cr(VI) to Cr(III) from wastewater and reuse for photocatalytic applications. *ACS Omega* 6, 35221–35243. <https://doi.org/10.1021/acsomega.1c00866>.
- Rabbani, A.W., Naz, G., Berdimurodov, E., Lal, B., Hosseini-bandegharai, A., 2023. Visible-light-driven photocatalytic properties of copper (I) oxide (Cu₂O) and its graphene-based nanocomposites 20, 1064–1077.
- Raizada, P., Thakur, P., Sudhaik, A., Singh, P., Thakur, V.K., Hosseini-Bandegharai, A., 2020. Fabrication of dual Z-scheme photocatalyst via coupling of BiOBr/Ag/AgCl heterojunction with P and S co-doped g-C₃N₄ for efficient phenol degradation. *Arab. J. Chem.* 13, 4538–4552. <https://doi.org/10.1016/j.arabjc.2019.10.001>.
- Rehman, M.S.U., Rashid, N., Ashfaq, M., Saif, A., Ahmad, N., Han, J.I., 2015. Global risk of pharmaceutical contamination from highly populated developing countries. *Chemosphere* 138, 1045–1055. <https://doi.org/10.1016/j.chemosphere.2013.02.036>.
- Ren, X., Meng, X., Ren, J., Tang, F., 2016. Graphitic carbon nitride nanosheets with tunable optical properties and their superoxide dismutase mimetic ability. *RSC Adv.* 6, 92839–92844. <https://doi.org/10.1039/c6ra21624b>.
- Salma, A., Thoröe-Boveleth, S., Schmidt, T.C., Tuerk, J., 2016. Dependence of transformation product formation on pH during photolytic and photocatalytic degradation of ciprofloxacin. *J. Hazard. Mater.* 313, 49–59. <https://doi.org/10.1016/j.jhazmat.2016.03.010>.
- Sarwar, A., Razaq, A., Zafar, M., Idrees, I., Rehman, F., Kim, W.Y., 2023. Copper tungstate (CuWO₄)/graphene quantum dots (GQDs) composite photocatalyst for enhanced degradation of phenol under visible light irradiation. *Results Phys.* 45, 106253. <https://doi.org/10.1016/j.rinp.2023.106253>.
- Sayed, M., Ismail, M., Khan, S., Tabassum, S., Khan, H.M., 2016. Degradation of ciprofloxacin in water by advanced oxidation process: kinetics study, influencing parameters and degradation pathways. *Environ. Technol.* 37, 590–602. <https://doi.org/10.1080/09593330.2015.1075597>.
- Schweitzer, L., Noblet, J., 2018. Water Contamination and Pollution. *Green Chem.* 20, 261–290. <https://doi.org/10.1016/B978-0-12-809270-5.00011-X>.
- Shanmugam, P., Smith, S.M., Boonyuen, S., Luengnarumitchai, A., 2023. In-situ development of boron doped g-C₃N₄ supported SBA-15 nanocomposites for photocatalytic degradation of tetracycline. *Environ. Res.* 224, 115496. <https://doi.org/10.1016/j.envres.2023.115496>.
- Shehu Imam, S., Adnan, R., Mohd Kaus, N.H., 2018. Photocatalytic degradation of ciprofloxacin in aqueous media: a short review. *Toxicol. Environ. Chem.* 100, 518–539. <https://doi.org/10.1080/02772248.2018.1545128>.
- Shen, Y., Xu, H., Zheng, Y., Wang, Y., Zhang, L., Zhang, Z., Zhong, L., He, Z., 2023. Fabrication of Bi/BiO(OH)/PVDF with improved photocatalytic activity for the degradation of ciprofloxacin. *Surf. Interfaces* 42, 103483. <https://doi.org/10.1016/j.surfin.2023.103483>.
- Sirés, I., Brillas, E., 2012. Remediation of water pollution caused by pharmaceutical residues based on electrochemical separation and degradation technologies: a review. *Environ. Int.* 40, 212–229. <https://doi.org/10.1016/j.envint.2011.07.012>.
- Sridharan, K., Jang, E., Park, T.J., 2013. Novel visible light active graphitic C₃N₄-TiO₂ composite photocatalyst: synergistic synthesis, growth and photocatalytic treatment of hazardous pollutants. *Appl. Catal. B* 142–143, 718–728. <https://doi.org/10.1016/j.apcatb.2013.05.077>.
- Tahir, M., Sherryana, A., Khan, A.A., Madi, M., Zerga, A.Y., Tahir, B., 2022. Defect engineering in graphitic carbon nitride nanotextures for energy efficient solar fuels production: a review. *Energy Fuel* 36, 8948–8977. <https://doi.org/10.1021/acs.energyfuels.2c01256>.
- Tian, Y., Chang, B., Fu, J., Zhou, B., Liu, J., Xi, F., Dong, X., 2014. Graphitic carbon nitride/Cu₂O heterojunctions: preparation, characterization, and enhanced photocatalytic activity under visible light. *J. Solid State Chem.* 212, 1–6. <https://doi.org/10.1016/j.jssc.2014.01.011>.
- Verlicchi, P., Al Aukidy, M., Zambello, E., 2012. Occurrence of pharmaceutical compounds in urban wastewater: removal, mass load and environmental risk after a secondary treatment-A review. *Sci. Total Environ.* 429, 123–155. <https://doi.org/10.1016/j.scitotenv.2012.04.028>.
- Vuggili, S.B., Gaur, U.K., Tyagi, T., Sharma, M., 2023. 2D/2D nitrogen-doped graphitic carbon nitride/cobalt sulfide nanostructures for fast photodegradation of methylene blue dye and real industrial sewage effluents. *Environ. Sci. Adv.* 795–814. <https://doi.org/10.1039/d2va00208f>.
- Wang, Z., Cai, X., Xie, X., Li, S., Zhang, X., Wang, Z., 2021. Visible-LED-light-driven photocatalytic degradation of ofloxacin and ciprofloxacin by magnetic biochar modified flower-like Bi₂WO₆: the synergistic effects, mechanism insights and degradation pathways. *Sci. Total Environ.* 764, 142879. <https://doi.org/10.1016/j.scitotenv.2020.142879>.

- Wen, X.J., Niu, C.G., Zhang, L., Liang, C., Guo, H., Zeng, G.M., 2018. Photocatalytic degradation of ciprofloxacin by a novel Z-scheme CeO₂-Ag/AgBr photocatalyst: influencing factors, possible degradation pathways, and mechanism insight. *J. Catal.* 358, 141–154. <https://doi.org/10.1016/j.jcat.2017.11.029>.
- Wen, S., Sang, L., Yang, G., He, X., Meng, J., Song, D., Yang, Y., 2023. In situ synthesis of silver-decorated defective graphitic carbon nitride for enhanced photocatalytic redox performance. *J. Alloy. Compd.* 962, 171194 <https://doi.org/10.1016/j.jallcom.2023.171194>.
- Wu, J., Cui, Y., Li, X., Khan, I., Liu, X., Xu, Y., Song, Y., Xie, H., 2023. Single-atom Pt anchored thiophene ring doped carbon nitride nanosheets for enhanced visible-light photocatalytic H₂ evolution and ciprofloxacin degradation. *Int. J. Hydrogen Energy.* <https://doi.org/10.1016/j.ijhydene.2023.07.175>.
- Wu, X., Gao, D., Wang, P., Yu, H., Yu, J., 2019. NH₄Cl-induced low-temperature formation of nitrogen-rich g-C₃N₄ nanosheets with improved photocatalytic hydrogen evolution. *Carbon N Y* 153, 757–766. <https://doi.org/10.1016/j.carbon.2019.07.083>.
- Wudil, Y.S., Ahmad, U.F., Gondal, M.A., Al-Osta, M.A., Almohammed, A., Sa'id, R.S., Hrahsheh, F., Haruna, K., Mohamed, M.J.S., 2023. Tuning of graphitic carbon nitride (g-C₃N₄) for photocatalysis: a critical review. *Arab. J. Chem.* 16 <https://doi.org/10.1016/j.arabjc.2023.104542>.
- Xia, P., Zhu, B., Yu, J., Cao, S., Jaroniec, M., 2017. Ultra-thin nanosheet assemblies of graphitic carbon nitride for enhanced photocatalytic CO₂ reduction. *J. Mater. Chem. A Mater.* 5, 3230–3238. <https://doi.org/10.1039/c6ta08310b>.
- Xu, B., Ahmed, M.B., Zhou, J.L., Altaee, A., Xu, G., Wu, M., 2018. Graphitic carbon nitride based nanocomposites for the photocatalysis of organic contaminants under visible irradiation: progress, limitations and future directions. *Sci. Total Environ.* 633, 546–559. <https://doi.org/10.1016/j.scitotenv.2018.03.206>.
- Xu, Y., Gao, S.P., 2012. Band gap of C₃N₄ in the GW approximation. *Int. J. Hydrogen Energy* 37, 11072–11080. <https://doi.org/10.1016/j.ijhydene.2012.04.138>.
- Xu, H., Wang, C., Song, Y., Zhu, J., Xu, Y., Yan, J., Song, Y., Li, H., 2014. CNT/Ag₃PO₄ composites with highly enhanced visible light photocatalytic activity and stability. *Chem. Eng. J.* 241, 35–42. <https://doi.org/10.1016/j.cej.2013.11.065>.
- Yu, J., Wang, K., Xiao, W., Cheng, B., 2014. Photocatalytic reduction of CO₂ into hydrocarbon solar fuels over g-C₃N₄-Pt nanocomposite photocatalysts. *PCCP* 16, 11492–11501. <https://doi.org/10.1039/c4cp00133h>.
- Zhang, S., Li, J., Wang, X., Huang, Y., Zeng, M., Xu, J., 2014. In situ ion exchange synthesis of strongly coupled Ag@AgCl/g-C₃N₄ porous nanosheets as plasmonic photocatalyst for highly efficient visible light photocatalysis. *ACS Appl. Mater. Interfaces* 6, 22116–22125. <https://doi.org/10.1021/am505528c>.
- Zhang, X., Xie, X., Wang, H., Zhang, J., Pan, B., Xie, Y., 2013. ChemInform abstract: enhanced photoresponsive ultrathin graphitic-phase C₃N₄ nanosheets for bioimaging. *ChemInform* 44, no-no. <https://doi.org/10.1002/chin.201320013>.
- Zhang, H., Xu, J., Yuan, Y., Guo, Y., Tan, X., Wang, H., Hu, X., Tang, C., 2024. Highly conductive Ti₃C₂ MXene reinforced g-C₃N₄ heterojunction photocatalytic for the degradation of ciprofloxacin: mechanism insight. *Sep. Purif. Technol.* 330 <https://doi.org/10.1016/j.seppur.2023.125520>.
- Zhao, J., Yang, Z., Yu, C., Qiu, J., Song, Z., 2018. Preparation of ultra-small molecule-like Ag nano-clusters in silicate glass based on ion-exchange process: energy transfer investigation from molecule-like Ag nano-clusters to Eu³⁺ ions. *Chem. Eng. J.* 341, 175–186. <https://doi.org/10.1016/j.cej.2018.02.028>.
- Zheng, Q., Durkin, D.P., Elenewski, J.E., Sun, Y., Banek, N.A., Hua, L., Chen, H., Wagner, M.J., Zhang, W., Shuai, D., 2016. Visible-light-responsive graphitic carbon nitride: rational design and photocatalytic applications for water treatment. *Environ. Sci. Tech.* <https://doi.org/10.1021/acs.est.6b02579>.
- Zheng, Y., Lin, L., Wang, B., Wang, X., 2015. Graphitic Carbon Nitride Polymers toward Sustainable Photoredox Catalysis. *Angew. Chem., Int. Ed. Engl.* 54, 12868–12884. <https://doi.org/10.1002/anie.201501788>.